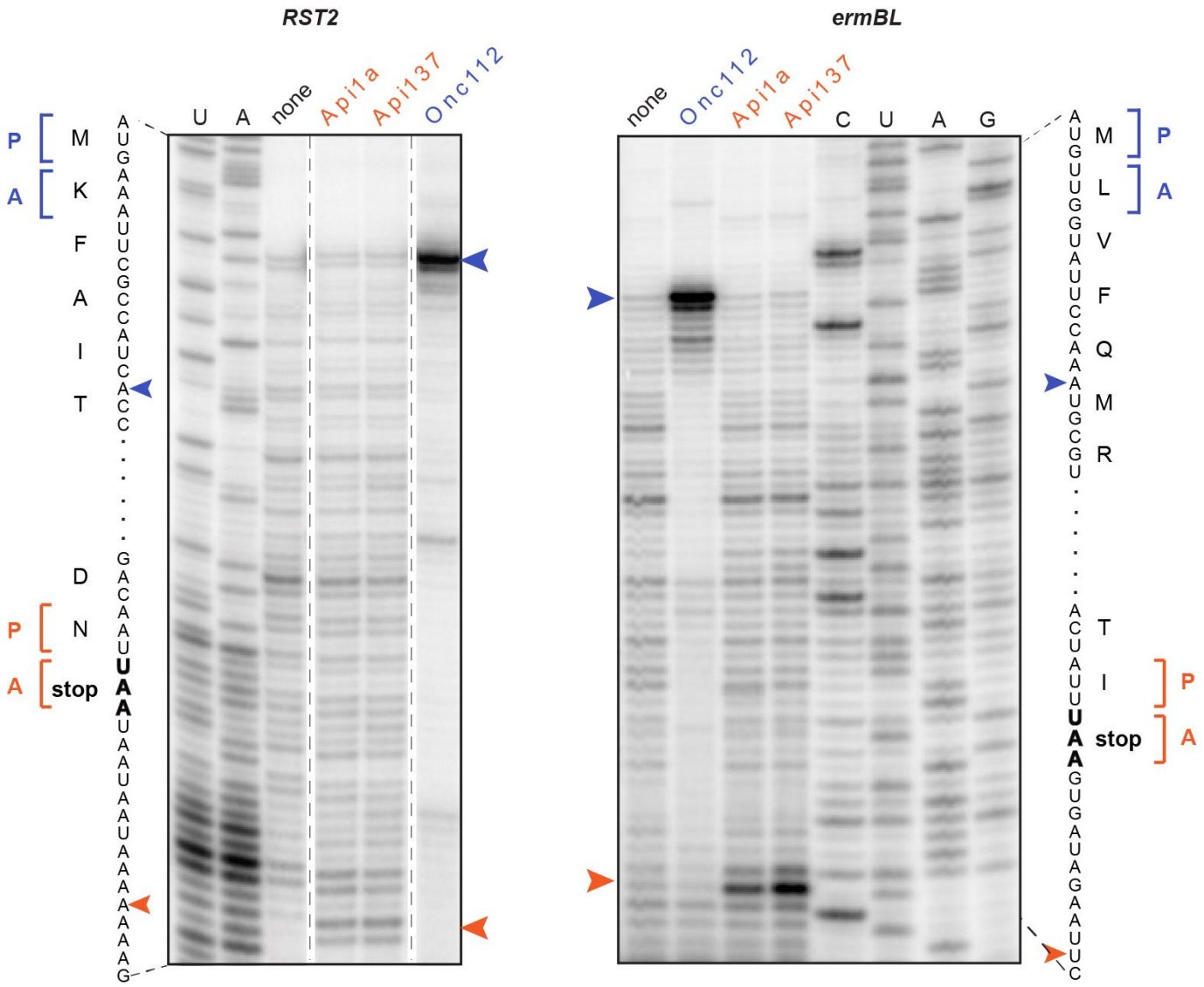

Supplementary Figure 1

Api137-induced ribosome stalling at the end of the ORFs

Toeprinting analysis of translation arrest in the synthetic ORF *RST2* (left) and the natural ORF *ermBL* (right) mediated by PrAMPs. The toeprint bands corresponding to the ribosomes arrested by Api137 or the natural apidaecin 1a (Api1a) at the stop codon of the ORF are indicated with orange arrowheads; the bands representing the ribosome arrested by Onc112 at the start codon are marked with blue arrowheads. Sequencing lanes are shown. The nucleotides corresponding to the toeprint bands are indicated in the gene sequence on the side of the gels; orange brackets indicate codons positioned in the P- and A- sites of the Api-stalled ribosome; blue brackets indicate codons in the P- and A- sites of the Onc112-stalled ribosome. The gels are representatives of two independent experiments.

a

E. coli strain		Minimal inhibitory concentration [μM]	Fold change
SQ171	wild type	12.5	
	23S rRNA: A2059C	100	8
	23S rRNA: A2503G	> 100	> 8
SQ110	wild type	12.5	
	SbmA: Ser251TAG (*)	> 100	> 8
	RF1: Asp241Gly (*)	> 100	> 8
BL21 (pZa-SbmA)	wild type	0.75	
	RF2: Arg262Cys (*)	> 100	> 128
	RF2: Gln280Leu (*)	50	64
	uL16: Arg81Cys (*)	6	8
AB301	wild type	12.5	
	uL4: Lys63Glu	> 100	> 8
	uL22: Δ_{82}MKR$_{84}$	> 100	> 8

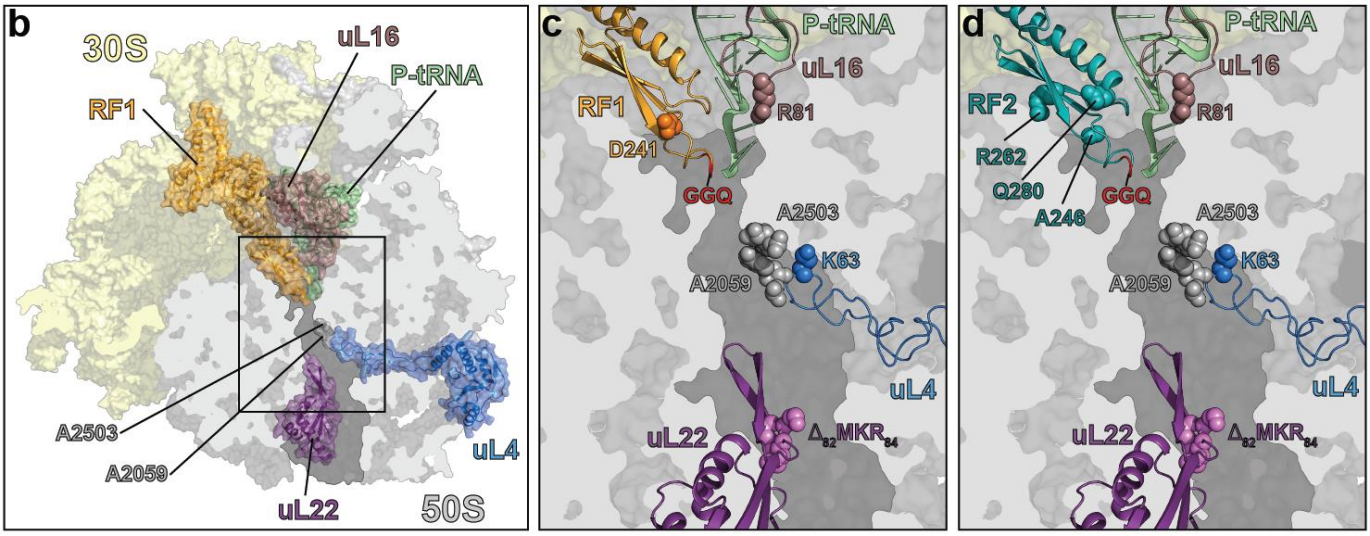

Supplementary Figure 2

Api137-resistance mutations.

a, Effect of the newly-isolated (marked by asterisks) or tested mutations on sensitivity of *E. coli* cells to Api137. The RF1 mutation is highlighted in orange; RF2 mutations, teal; rRNA mutations. grey; uL16, brown; uL4, blue; uL22, purple. Each MIC was determined in at least two independent experiments. **b-d**, Location of resistance mutations within the context of the terminating ribosome. **b**, Transverse section of the 50S ribosomal subunit (grey) of the 70S ribosome (30S subunit, yellow) showing the location of ribosomal proteins uL4, uL16, uL22 or 23S rRNA nucleotides (grey) whose mutations confer resistance to Api137. The region enlarged in (**c**) is boxed. **c-d**, Location of Api137 resistance mutations (spheres) in 23S rRNA (grey), ribosomal proteins uL4 (blue), uL16 (brown) and uL22 (purple), as well as (**c**) RF1 (orange) or (**d**) RF2 (teal). The GGQ motif of RF1 and RF2 is colored red in (**c**) and (**d**).

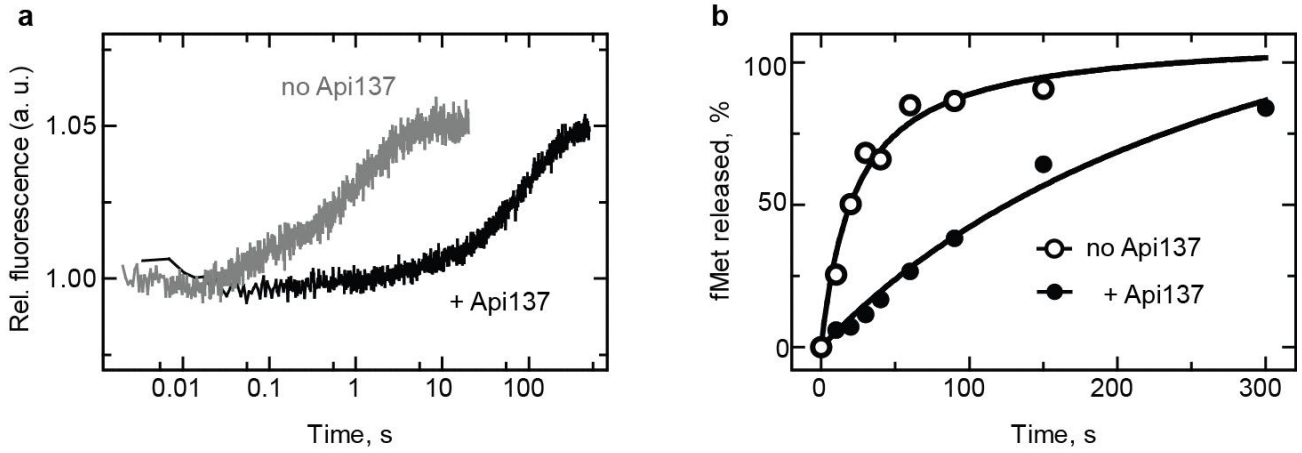

Supplementary Figure 3

Mutations allow faster dissociation of RF1 and RF2 from the PostHC.

a, Dissociation of RF1(D241G) from the PostHC in the presence of Api137**.** RF1(D241G)$_{Qsy}$ was incubated with PreHC$_{Flu}$ (0.05 μM) to generate PostHC$_{Flu}$ and then mixed with a 10-fold excess of unlabeled RF1 and RF3·GTP in the absence (grey) or in the presence (black) of Api137 (1 μM). The traces represent the average of up to eight technical replicates. No dissociation of wt RF1 in the presence of Api137 was observed under the same experimental conditions (Fig. 2f). **b**, Peptide hydrolysis by K12 strain-specific RF2(Ala246Thr) at turnover conditions in the absence (open circles) or in the presence (closed circles) of Api137 (1 μM). In the presence of Api137, the peptide hydrolysis reaction proceeds faster when it is catalyzed by the K12 strain RF2, compared to the B strain RF2 (Fig. 2c).

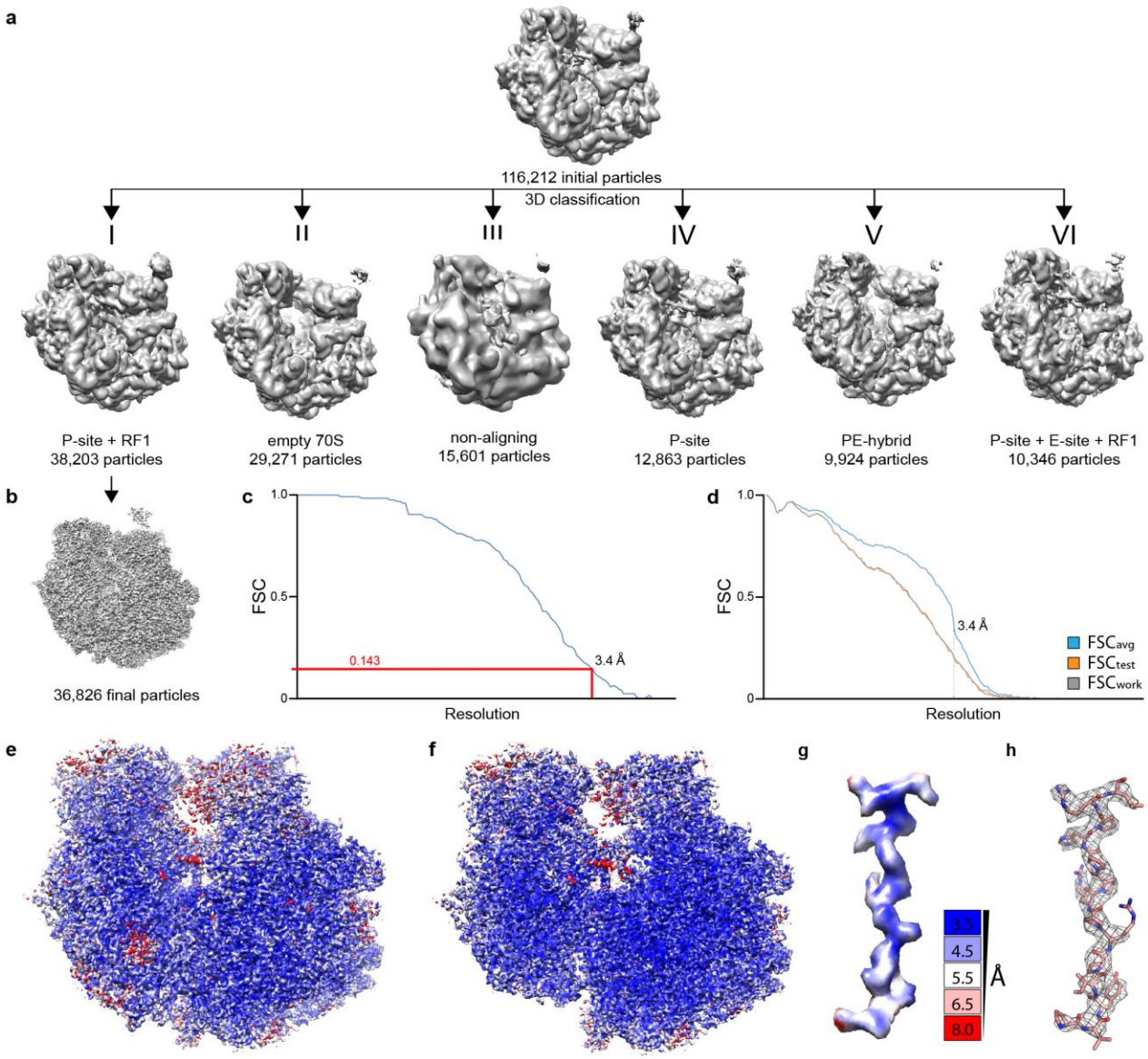

Supplementary Figure 4

In silico sorting and resolution of the Api-RF1-70S complex.

a, *In silico* sorting was performed with the FreAlign 9.11 software package (as described in Grigorieff, N., *J. Struct. Biol.* **157**, 117-125 (2007)). Initial alignment of 116,212 particles was followed by 3D classification, resulting in six different classes. Class 1 (38,203 particles) was further refined, yielding a (**b**) final reconstruction consisting of 36,826 particles, with (**c**) an average resolution of 3.4 Å (based on the Fourier shell correlation (FSC) curve at FSC 0.143). **d**, Validation of the fit of molecular models to cryo-EM map for the Api137-RF1-70S complex. FSC curves calculated between the refined model and the final map (blue), with the self- and cross-validated correlations in orange and black, respectively. Information beyond 3.4 Å was not used during refinement and preserved for validation. (**e**) Side view and (**f**) transverse section of the cryo-EM map of Api137-RF1-70S complex colored according to local resolution as shown previously (Kucukelbir, A., Sigworth, F. J. & Tagare, H. D., *Nat. Methods* **11**, 63-65 (2014)). **g-h**, Cryo-EM density for Api137 (**g**) colored according to local resolution and (**h**) shown as grey mesh with molecular model for residues 5-18.

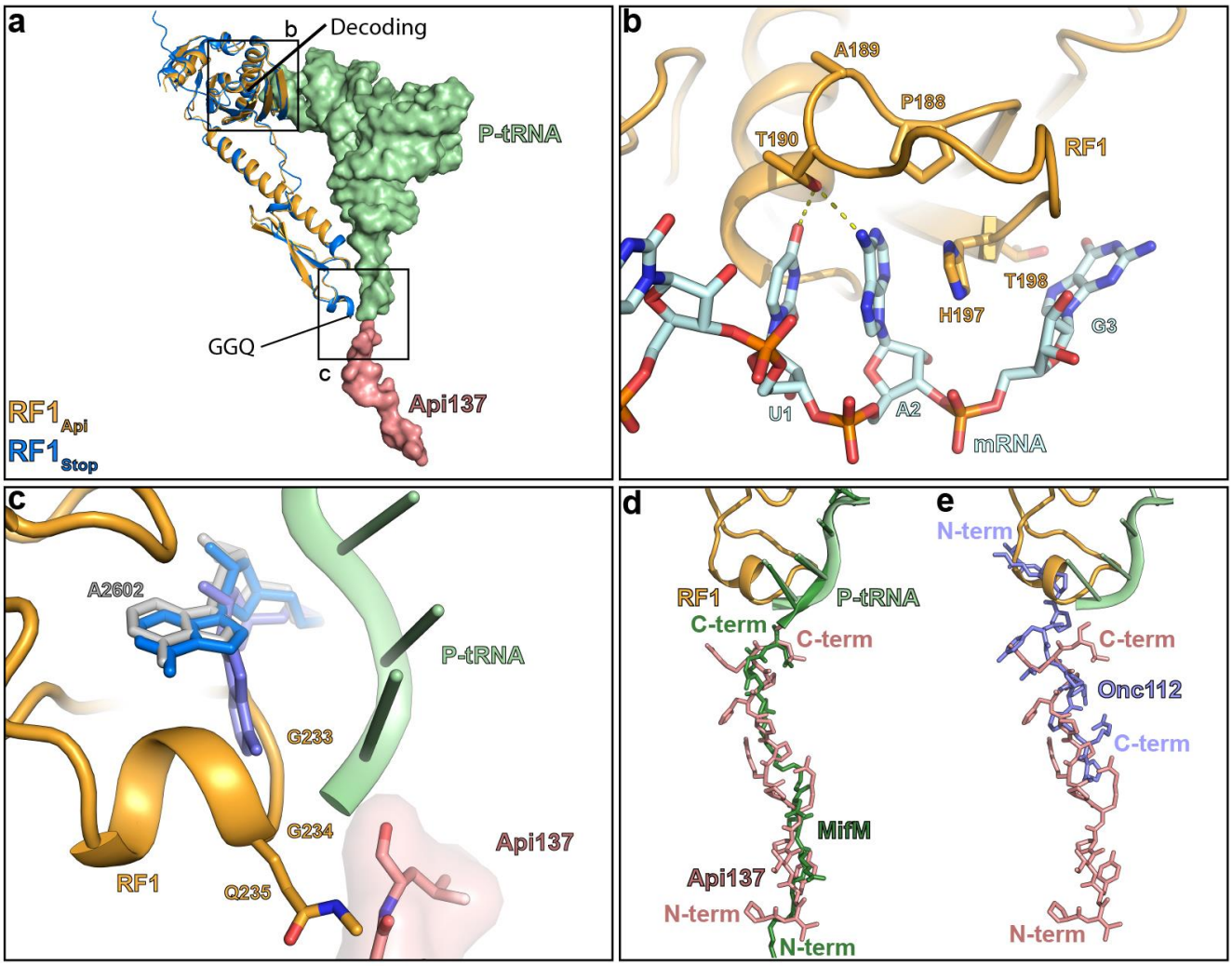

Supplementary Figure 5

Features of the Api137-RF1-70S complex.

a, RF1 (orange), deacylated P-site tRNA (green) and Api137 (salmon) in the Api137-RF1-70S complex. The position of RF1 during canonical termination is shown in blue (PDBID 5J30; Pierson, W. E. *et al., Cell Rep.* **17**, 11-18 (2016)). Boxed regions are zoomed in the panels (**b**) and (**c**). **b**, Interaction of the PAT motif of RF1 (orange) with the UAG stop codon of the mRNA (cyan) in the Api137-RF1-70S complex. **c**, A2602 of the 23S rRNA is in the rotated conformation as observed in previous RF1-70S structures (Korostelev, A. *et al.*, *EMBO J.* **29**, 2577-2585 (2010); Pierson, W. E. *et al., Cell Rep.* **17**, 11-18 (2016); Laurberg, M. *et al., Nature* **454**, 852-857 (2008); Svidritskiy, E. & Korostelev, A. A., *Structure* **23**, 2155-2161 (2015)). Conformation of A2602 (grey) in Api137-RF1-70S complex compared to A2602 (blue) during canonical termination (PDBID 5J30; Pierson, W. E. *et al., Cell Rep.* **17**, 11-18 (2016)) and A2602 (slate) from the pre-attack state (PDBID 1VY4; Polikanov, Y. S., Steitz, T. A. & Innis, C. A., *Nat. Struct. Mol. Biol.* **21**, 787-793 (2014)). Api137 (salmon) and P-site tRNA (green) are shown for reference. **d, e**, The binding position of Api137 (salmon) relative to the (**d**) MifM nascent chain (dark green; Sohmen, D. *et al.*, *Nat. Commun.* **6**, 6941 (2015)) or (**e**) antimicrobial peptide Onc112 (slate; Seefeldt, A. C. *et al., Nat. Struct. Mol. Biol.* **22**, 470-475 (2015)). In (**d**) and (**e**) the orientations of the peptides are indicated.

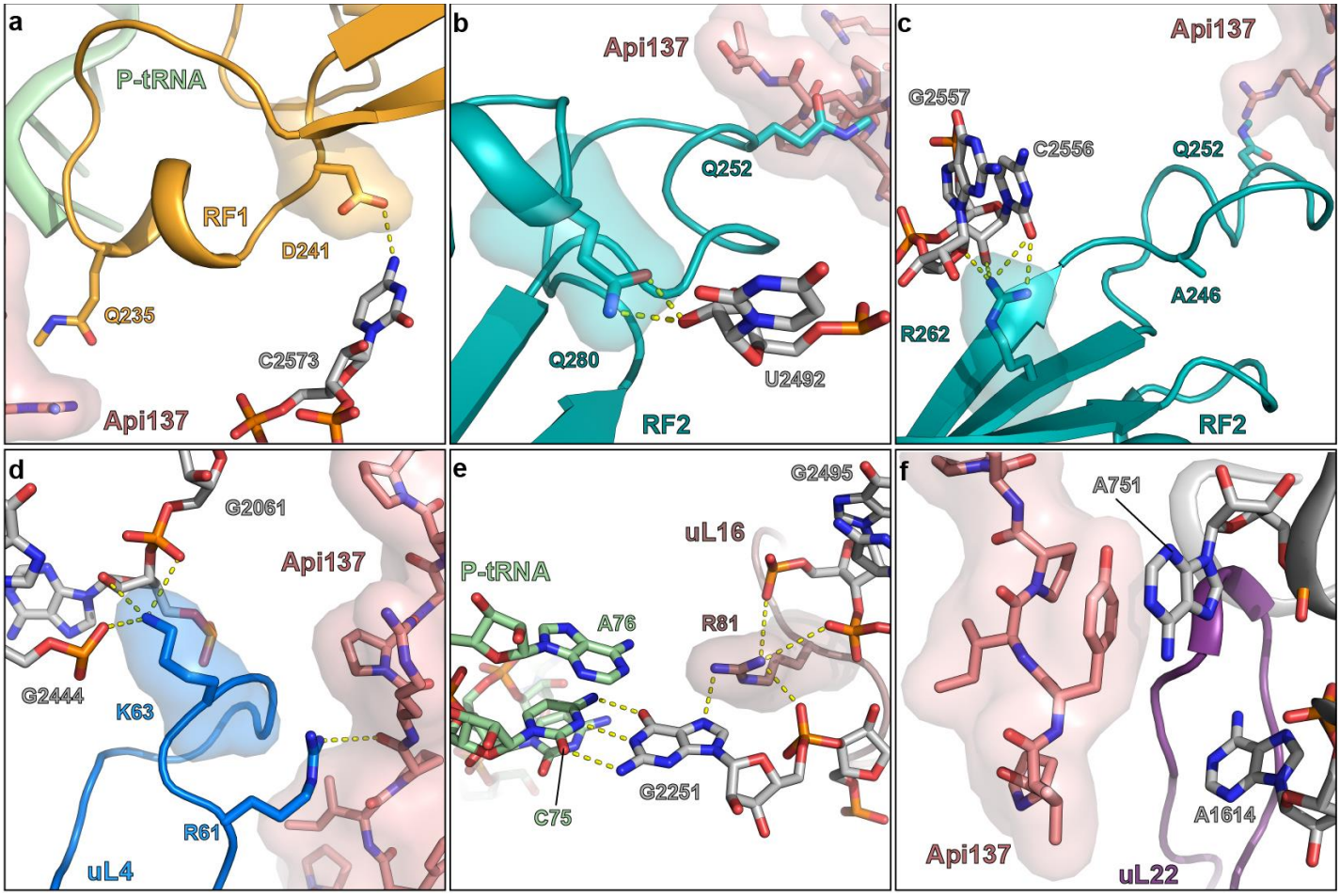

Supplementary Figure 6

Mutations that increase resistance to Api137

(**a-c**) Location of residues in (**a**) RF1 (orange) and (**b, c**) RF2 (teal) that increase resistance to Api137 when mutated. Site of mutations are shown in stick and surface representation and glutamines of the GGQ motif (Gln235 in RF1 and Gln252 in RF2) are shown as sticks for reference. (**d-f**) Location of Api137 resistance mutations in ribosomal proteins. (**d**) Lys63 in uL4 (blue) interacts with 23S rRNA residues G2061 and G2444. (**e**) Deletion of $_{82}$MKR$_{84}$ (outside of the figure boundaries) in uL22 (purple) confers resistance to Api137 presumably by changing the geometry of the uL22 exit tunnel loop and disrupting Api137 interaction with neighboring 23S rRNA nucleotides (grey), such as A751. (**f**) The mutation of Arg81 in uL16 (brown) may relieve Api137-mediated RF1 and RF2 trapping by indirectly destabilizing interactions of deacylated tRNA with the P-site mediated by G2251 of the 23S rRNA.

Supplementary Table 1. Deletion of the RF3-encoding *prfC* gene affects minimal inhibitory concentration (MIC) of Api137

***E. coli* strain**	**MIC [µM]**
wild type (BW25113) [a)]	6.25
Δ*xylA* [b)]	6.25
Δ*prfC* [c)]	0.75

[a)] Parental *E. coli* K-type strain
[b)] The *xylA::kan* strain, where an unrelated gene was inactivated, was used as an additional negative control
[c)] The *prfC::kan* strain

Supplementary Table 2: DNA & RNA templates

Promoter – blue, ORF – red, annealing site for toeprinting primer – purple, annealing site for oligonucleotide for RNase H treatment of disomes – green. Start codons of the ORFs are shown in bold, stop codons are underlined.

Name	DNA Sequence (5' – 3')
yrbA-fs	TAATACGACTCACTATAGGGCTTAAGTATAAGGAGGAAAACAT**ATG**AT ATACCCCTGCGGAGTGGGCGCGCGATCGCAAACTGAACGGCTTTAG GCCGACCTCGACAGTTGGATTCACGTGCTGAATCCTGATGCGATGTC GAGTTAATAAGCAAAATTCATTATAACC
ermCL-UAG	TTAATACGACTCACTATAGGGAATTGTGAGCGGATAACAATTGCTAGT CTTAAGTTTTATAAGGAGGAAAAAAT**ATG**GGCATTTTTAGTATTTTTGT AATCAGCACAGTTCATTATCAACCAAACAAAAAATAGGTGGTTATAATG AATCGTTAATAAGCAAAATTCATTATAACCAAATTAAAGAGGGTTATAA
RST2	TAATACGACTCACTATAGGGCTTAAGTATAAGGAGGAAAACAT**ATG**TA TTGGGTAACCTCACGTCAGCCGAATATGCTGAAAATCCATGGCTTCGA AGACTGCGCCTAATAATAATAAAAAAAGTGATAGAATTCTATCGTTAAT AAGCAAAATTCATTATAACC
ermBL	TAATACGACTCACTATAGGGCTTAAGTATAAGGAGGAAAAAAT**ATG**TT GGTATTCCAAATGCGTAATGTAGATAAAACATCTACTATTTAAGTGATA GAATTCTATCGTTAATAAGCAAAATTCATTATAACC
Start-Stop	GGCAAGGAGGUAAAUA**AUG**UAAACGAUU
tnaC-UAG	ACATGGATTCTTGACAATTAATCATCGGCTCGTATAATGTGTGGAAGTT TTATAAGGAGGAAAACAT**ATG**AATATCTTACATATATGTGTGACCTCAA AATGGTTCAATATTGACAACAAAATTGTCGATCACCGCCCTTAG
tnaC-UGA	ACATGGATTCTTGACAATTAATCATCGGCTCGTATAATGTGTGGAAGTT TTATAAGGAGGAAAACAT**ATG**AATATCTTACATATATGTGTGACCTCAA AATGGTTCAATATTGACAACAAAATTGTCGATCACCGCCCTTGA
2XermCL_S10_ UAG	UAAUACGACUCACUAUAGGGAGUUUUAUAAGGAGGAAAAAAU**AUG**G GCAUUUUUAGUAUUUUUGUAAUCUAGACAGUUCAUUAUCAACCAAA CAAAAAAUAAAGUUUUAUAAGGAGGAAAAAAU**AUG**GGCAUUUUUAGU AUUUUUGUAAUCUAGACAGUUCAUUAUCAACCAAACAAAAAAUAA

Supplementary Table 3: DNA primers used in this study

Name	Sequence
T7-IR-AUG	TAATACGACTCACTATAGGGCTTAAGTATAAGGAGGAAAACATATG
IR-yrbA-fs15-RF1	GTATAAGGAGGAAAACATATGATATACCCCTGCGGAGTGGGCGCGCGATCGCAAACTGAACGGCTTTAGGCCGACCTCGACAGTTGGAT
posT-NV1	GGTTATAATGAATTTTGCTTATTAACTCGACATCGCATCAGGATTCAGCACGTGAATCCAACTGTCGAGGTCG
T7	TAATACGACTCACTATAGGG
ermCL-UAG	TTATAACCCTCTTTAATTTGGTTATAATGAATTTTGCTTATTAACGATTCATTATAACCACCTATT
ermCL-TP-term	TTATAACCCTCTTTAATTTGGTT
SbmA-seq-fwd	CATTTGGCTGACGCTTTGTA
SbmA-seq-rev	TACTACACCCCGCTAAAACC
SbmA-EcoRI-rev	TGACGCGCGGAATTCCTTCT
PrfA-seq-fwd	CTGAATATTCTGCGCGACAG
PrfA-seq-rev	CAGGATTTCAGCATCACGC
PrfB-seq-fwd	GCTCTTATCACCGCATTTTG
PrfB-seq-rev	GTTCATTGTTAAGATCGACTACC
PrfC-seq-fwd	GAAGGTAAGCTGGATATGCTG
PrfC-seq-rev	GCTTCTGATAACGTAGCCAG
rplP-seq-fwd	CGTTAAAGTGTGGATCTTCAAAGG
rplP-seq-rev	CACTTGCTTCAACAGGTGAG
L2667	GGTCCTCTCGTACTAGGAGCAG
L2180	GGGTGGTATTTCAAGGTCGG
Ptrc-tnaC	ACATGGATTCTTGACAATTAATCATCGGCTCGTATAATGTGTGGAAGTTTTATAAGGAGGAAAACATATG
tnaC-UAG-rev	GCAAACTAAGGGCGGTGATCGAC
tnaC-UGA-rev	GCAAATCAAGGGCGGTGATCGAC

Supplementary Table 4: Bacterial strains used in this study

***E. coli* strain**	**Type**	**Source**
SQ171	K-strain; F-, *Δ(rrsH-aspU)794(::FRT)*, *λ*$^-$, *Δ(rrfG-rrsG)791(::FRT)*, *Δ(rrfF-rrsD)793(::FRT)*, *rph-1*, *Δ(rrsC-trpT)795(::FRT)*, *Δ(rrsA-rrfA)792(::FRT)*, *Δ(rrsB-rrfB)790(::FRT)*, *Δ(rrsE-rrfE)789(::FRT)*, ptRNA67, pKK3535	Quan, S. *et al*., *G3* **5**, 2555-2557 (2015)
SQ110	K-strain, F-, *Δ(rrsH-aspU)794(::FRT)*, *λ*$^-$, *Δ(rrfG-rrsG)791(::FRT)*, *Δ(rrfF-rrsD)793(::FRT)*, *rph-1*, *Δ(rrsC-trpT)795(::FRT)*, *Δ(rrsA-rrfA)792(::FRT)*, *Δ(rrsB-rrfB)790(::FRT)*, ptRNA67	Quan, S. *et al*., *G3* **5**, 2555-2557 (2015)
SQ110 ApiR2	derived from SQ110, *sbmA*(C752A)	*this study*
SQ110 ApiR21	derived from SQ110, *prfA*(A722G)	*this study*
BL21 (DE3)	B-strain; F-, *lon-11*, *Δ(ompT-nfrA)885*, *Δ(galM-ybhJ)884*, *λDE3 [lacI, lacUV5-T7 gene 1, ind1, sam7, nin5]*, *Δ46*, *[mal*$^+$*]*$_{K\text{-}12}$(λ^S), *hsdS10*	Wood, W.B., *J Mol Biol* **16**, 118-133 (1966); Studier, F.W. & Moffatt, B.A., *J Mol Biol* **189**, 113-30 (1986)
BL21 ApiR10	derived from BL21 (DE3), *rplP*(G241A), pZα-SbmA	*this study*
BL21 ApiR11	derived from BL21 (DE3), *prfB*(C784T), pZα-SbmA	*this study*
BL21 ApiR12	derived from BL21 (DE3), *prfB*(A839T), pZα-SbmA	*this study*
AB301	K-strain; Hfr(PO21), *relA1*, *spoT1*, *metB1*	Bouck, N. & Adelberg, E.A., *J Bacteriol* **102**, 688-701 (1970)
N281	K-strain; Hfr(PO21), *relA1*, *rplV281*, *spoT1*, *metB1*	Wittmann, H.G. *et al*., *Mol Gen Genet* **127**, 175-89. (1973); Chittum, H.S. & Champney, W.S., *J Bacteriol* **176**, 6192-8 (1994).
N282	K-strain; Hfr(PO21), *relA1*, *rplD282*, *spoT1*, *metB1*	Wittmann, H.G. *et al*., *Mol Gen Genet* **127**, 175-89. (1973); Chittum, H.S. & Champney, W.S., *J Bacteriol* **176**, 6192-8 (1994).
SQ171-Δ*tolC*	derived from SQ171; Δ*tolC*, pCSacB	Kannan, K., Vázquez-Laslop, N. & Mankin, A.S., *Cell* **151**, 508-520 (2012)
SQ171-Δ*tolC*/W3	derived from SQ171-Δ*tolC*, *lacZ(*C2035T) pCSacB	*this study*
BW25113	F-, *Δ(araD-araB)567*, *ΔlacZ4787*(::rrnB-3), *λ*$^-$, *rph-1*, *Δ(rhaD-rhaB)568*, *hsdR514*	Baba, T. *et al.*, *Mol Syst Biol* **2**, 2006 0008 (2006)
BW25113 Δ*xylA* (JW3537)	F-, *Δ(araD-araB)567*, *ΔlacZ4787*(::rrnB-3), *λ*$^-$, *ΔxylA748::kan*, *rph-1*, *Δ(rhaD-rhaB)568*, *hsdR514*	Baba, T. *et al.*, *Mol Syst Biol* **2**, 2006 0008 (2006)
BW25113 Δ*prfC* (JW5873)	F-, *Δ(araD-araB)567*, *ΔlacZ4787*(::rrnB-3), *λ*$^-$, *rph-1*, *Δ(rhaD-rhaB)568*, *hsdR514*, *ΔprfC770::kan*	Baba, T. *et al.*, *Mol Syst Biol* **2**, 2006 0008 (2006)